Appl. Phys. B 65, 137–150 (1997)

Applied Physics B Lasers and Optics

Invited paper

Semiconductor saturable absorber mirrors supporting sub-10-fs pulses

I.D. Jung[1], F.X. Kärtner[1], N. Matuschek[1], D.H. Sutter[1], F. Morier-Genoud[1], Z. Shi[1], V. Scheuer[2], M. Tilsch[2], T. Tschudi[2], U. Keller[1]

[1] Ultrafast Laser Physics, Institute of Quantum Electronics, Swiss Federal Institute of Technology, ETH Honggerberg - HPT, CH - 8093 Zürich, Switzerland
[2] Institute for Applied Physics, TH Darmstadt, Germany

Received: 18 March 1997/Revised version: 12 May 1997

Abstract. We generated self-starting sub-10-fs pulses from a Ti:sapphire laser using a combination of a broadband semiconductor saturable absorber mirror (SESAM), novel double-chirped mirrors, and Kerr-lens modelocking. We present a detailed overview of broadband SESAMs used in Ti:sapphire lasers and discuss their design issues. Using such a SESAM to assist the KLM process, we have generated pulses with a duration of only 6.5 fs, the shortest to date directly from the laser. Pulses as short as 13 fs were generated by soliton modelocking alone. Higher-order dispersion compensation was achieved with novel double-chirped mirrors in combination with intracavity prisms.

PACS: 42.60F; 42.65; 42.80

The many potential applications of ultrashort laser pulses in physics, chemistry, biology, or medicine have strongly motivated the intensive work in this field over the past few years [1]. The applications benefit from either the time resolution, the high peak power, or the broad coherent spectrum of femtosecond pulses. For example, heavy–light-hole quantum beats in bulk GaAs have been studied with 20-fs time resolution [2]. Sub-20-fs ultraviolet pulses can be efficiently generated due to the high peak power of amplified ultrashort pulses of Ti:sapphire laser systems [3]. Furthermore, the efficiency of high-harmonic generation is larger for shorter pulses [4, 5]. A broad coherent spectrum is required for femtosecond optical pulse shaping and processing (i.e. "coherent control"), which provides an attractive experimental tool for more sophisticated ultrafast spectroscopy [6]. Such coherent control can also contribute to a wide range of communications and information processing applications, such as high-density wavelength-division multiplexing [7], interconnects and networking [8]. In addition, optical coherence tomography benefits from the short coherence length and the broad spectral bandwidth of ultrashort pulses [9]. The number of applications in the sub-50-fs pulse regime continues to increase, stimulated by the improvements in ultrafast sources. The shortest pulses currently generated directly out of a laser have a pulse duration of 6.5 fs at 200 mW average output power [10]. Even shorter pulses of ≈ 5 fs have been obtained by external pulse compression [11, 12]. In addition, passively modelocked diode-pumped solid-state lasers are beginning to provide compact femtosecond sources in the visible and near-infrared wavelength range [13].

The currently shortest pulses of 6.5 fs obtained directly from a Ti:sapphire laser [10] are still not at the theoretical limit, which is around 3 fs for Ti:sapphire. The goal to push towards this theoretical limit may not appear very attractive. However, this push for ever-shorter pulses often results in new and important developments, which benefit not only the ultimate limits in ultrashort-pulse generation, but also lead to more reliable, versatile, and compact femtosecond sources. Examples of such developments include novel modelocking techniques such as Kerr-lens modelocking (KLM) [14–17], soliton modelocking [18–20], chirped mirrors for dispersion compensation [21, 22], and semiconductor saturable-absorber mirrors (SESAMs) [13, 23]. These developments provide the basis for increasingly simpler ultrafast lasers, allowing for their use in new applications that do not necessarily require a laser expert to operate the ultrafast system.

It is well known that higher-order dispersion is the major limitation in short-pulse generation [24, 25]. In Ti:sapphire lasers, the intracavity prism pair [26], which is well established for compensating the group delay dispersion (GDD), is mainly responsible for this higher-order dispersion. Sub-10-fs pulses were obtained for the first time by minimizing all dispersive effects in the laser cavity by using low dispersive material for the prisms, a short laser crystal, and silver mirrors [25]. A new solution to the problem of dispersion compensation was provided by the invention of chirped mirrors [21, 27, 28]. These mirrors offer negative GDD and a larger spectral bandwidth than standard laser mirrors. Pulses as short as ≈ 7.5 fs have been generated by using chirped mirrors instead of prism pairs in a Ti:sapphire ring laser [29]. However, the prisms are still a very useful element in the laser. For practical applications it is often very helpful that the laser can be easily converted from generating extremely short pulses into a widely tunable source even at the expense of the pulse duration. We generated self-starting 6.5-fs pulses by using prism pairs in combina-

tion with a double-chirped mirror [10, 22]. These mirrors were designed to compensate the higher-order GDD of the prism pair. Self-starting was obtained by using a broadband SESAM [30].

The use of SESAMs in the Ti:sapphire laser is another new development arising from the need for a reliable starting mechanism for ultrashort pulses. Until recently, the shortest pulses were generated by KLM alone [25, 29, 30]. However, pure KLM pulses are typically not self-starting in the 10-fs regime. This is not surprising, since in a 10-fs Ti:sapphire laser with a 100-MHz repetition rate, the peak power changes by 6 orders of magnitude when the laser switches from cw to pulsed operation. Therefore, nonlinear effects that are strong in the sub-10-fs regime are typically too small to initiate modelocking in the cw-operation regime. Broadband SESAMs, which have been designed especially for Ti:sapphire lasers [30], now offer the possibility to start KLM for pulses below 10-fs duration. Furthermore, the SESAMs relax the critical cavity alignment, which is necessary to obtain a strong and optimized KLM, because even a SESAM with a moderate amount of saturable absorption will drive the pulsewidth down to typically about 100 fs on its own. SESAMs have been successfully used to passively modelock many solid-state lasers such as Nd:YLF [23, 32–34], Nd:YAG [33, 35], Nd:LSB [36], Nd:YVO_4 [34], Nd:glass [37, 38], Yb:YAG [39], Yb:glass [40], Cr:LiSAF [41–46], Cr:YAG [47, 48], Cr:forsterite [49], and others. SESAMs can also provide self-starting, stable modelocking in lasers that are difficult or problematic for KLM, such as diode-pumped lasers with a weak Kerr nonlinearity [46].

We have also found and described a new modelocking technique, which we refer to as soliton modelocking [18–20]. The main difference between KLM and soliton modelocking can be found in the temporal behaviour of the saturable-absorber action. KLM is an artificial fast saturable absorber, whereas soliton modelocking is based on a slow saturable absorber realized by the SESAM. Soliton modelocking has been experimentally verified in Ti:sapphire lasers [19]. Pulses as short as 13 fs have been generated with a purely soliton-modelocked Ti:sapphire laser by using a broadband SESAM [20]. The SESAM used for the 13-fs result shows a recovery time of 60 fs, which is more than four times longer than the pulsewidth. However, stable pulses can still be obtained, because the pulse shaping is done by soliton formation, whereas the absorber only starts and stabilizes the pulse. In contrast to KLM, soliton modelocking is obtained over the full cavity stability regime of the laser cavity.

Depending on the temporal behavior of the SESAM and the final pulsewidth, the essential modelocking mechanism in solid-state lasers is either fast saturable-absorber modelocking [50] or a continuous transition to soliton modelocking stabilized by a slow saturable absorber [18, 20]. In combination with diode pumping, SESAMs offer the realization of compact and reliable ultrafast laser sources.

In the following two sections, we discuss the ideal modelocking mechanism, the ideal saturable absorber and compare them with mechanisms that are available today. Section 3 describes the experiments resulting in the shortest pulse, which arose because of major progress in dispersion compensation and the fabrication of broadband SESAMs.

1 Modelocking techniques

The generation of ultrashort pulses relies on passive modelocking techniques, because only a passive shutter is fast enough to shape and stabilize ultrashort pulses. The passive shutter is obtained from a saturable absorber, which can be either a real absorber such as semiconductors and dyes or an artificial absorber created by the modelocking mechanism. In this section, we critically review the desired absorber properties needed to generate self-starting pulses in the sub-10-fs regime and ask how these parameters compare with existing saturable absorbers. We distinguish between two existing modelocking mechanisms in Ti:sapphire lasers which are capable of generating pulses in the 10-fs pulse regime. These modelocking mechanisms are Kerr-lens modelocking and soliton modelocking. The latter is based on a slow saturable absorber made of a SESAM.

KLM has proven to be an excellent modelocking mechanism based on the generation of an artificial fast saturable absorber (Fig. 1a) [14–17, 51]. The Kerr nonlinearity of the Ti:sapphire crystal causes a strong self-focusing of the laser

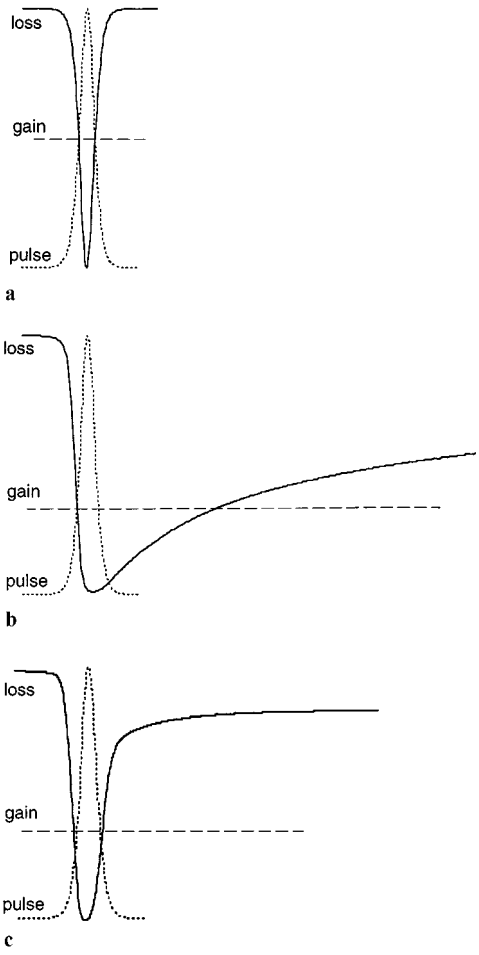

Fig. 1a–c. Pulse-shaping and stabilization mechanisms in a Ti:sapphire laser for use of **a** the fast artificial saturable absorber KLM, **b** the slow saturable absorber given by the response of a SESAM plus soliton formation, **c** the response of a SESAM and a fast contribution due to KLM. The loss consists of the frequency-independent loss of the saturable absorber and the output coupler, but does not contain the losses introduced by gain filtering or other intracavity filtering elements

Table 1. Comparison of different modelocking mechanisms with the ideal modelocker for sub-10-fs pulse generation

characteristics	ideal	pure KLM without SESAM	soliton modelocking with SESAM
modulation depth	high	can be high	partly adaptable
nonsaturable losses	none	soft aperture: none hard aperture: possible	material/mirror losses
saturation behavior	adaptable	unknown	adaptable
absorber recovery time with respect to			bitemporal
pulse shortening	fast	fast	slow
self-starting	slow	fast	slower
wavelength dependence	no	no	yes
spatio-temporal coupling	no	yes	no
cavity design	full freedom	critical alignment	no critical alignment

beam inside the crystal. This results in an overall change in the beam size. Therefore, the self-focusing of the beam leads to a self-amplitude modulation in conjunction with either a hard or a soft aperture. The pulsed mode of operation is favoured, because it experiences less losses than the cw mode because of the aperture. We have demonstrated that modelocking of Ti:sapphire lasers in the 10-fs regime is also possible by soliton modelocking, stabilized by a broadband SESAM [30]. Soliton modelocking is a modelocking mechanism in which the pulse is completely shaped by soliton formation, but stabilized by a slow saturable absorber. In contrast to KLM, the net-gain window does not close immediately after passage of the pulse (Fig. 1b). If the modulation depth of the saturable absorber is high enough, it is still possible to generate short pulses. Self-phase modulation (SPM) and GDD are in balance only for the soliton. Any background noise or fluctuations that may grow, do not experience SPM, but rather GDD. They are spread in time as a result of the GDD and are ultimately absorbed by the slowly recovering absorber. Such a slow absorber can be obtained by a broadband SESAM, which is an independently adjustable element in the laser cavity.

In Table 1, we define the characteristics of an ideal modelocking mechanism and make a comparison with the two modelocking regimes described above. Furthermore, we assume that dispersion compensation is a problem that can be treated separately, and that the gain bandwidth is as broad as that of a Ti:sapphire laser extending from about 650 nm to 1050 nm. Afterwards, we explicitly ask what would be the ideal absorber for generating the theoretically shortest pulses out of a Ti:sapphire laser.

1.1 Modulation depth

The modulation depth is the total amount of saturable losses of the absorber, which can be bleached by an "infinitely" high pulse energy (i.e. a pulse energy density much larger than the saturation fluence of the absorber). According to all modelocking theories [50, 52, 53], we find that the pulsewidth τ_p is typically inversely proportional to the modulation depth $\Delta R \approx 2q_0$ of the saturable absorber:

$$\tau_p \propto \frac{1}{q_0^{\alpha}}, \qquad \text{with } \alpha > 0\,. \tag{1}$$

The exponential factor α varies in the different modelocking theories. A high modulation depth always helps to achieve shorter pulses. In KLM, the modulation depth is produced either by the decreased losses because of self-focusing through a hard aperture, or by the increased gain in the laser as a result of an increased overlap of the laser mode with the pump mode in the laser crystal. We observe that the output power of a 10-fs-KLM laser system is typically reduced by a factor of 2 when the laser switches from the pulsed into the cw mode. The modulation depth is then as large as the total losses if we assume operation far above threshold. For instance, a modulation depth of about 10% can be obtained if the laser is operated several times above threshold via a 10% output coupler and soft-aperture KLM. In soliton modelocking, we can change the modulation depth of the absorber to within a range of a few percent by choosing a suitable absorber material, absorber thickness and structure of the SESAM. Numerical simulations show that we need about 10% modulation depth and more to maintain sub-10-fs pulses depending on the details of the bandwidth limitation in the system. A large modulation depth over the full bandwidth of the pulse spectrum is desirable. This is not a trivial task, because the saturable absorption of semiconductors is wavelength dependent, as will be discussed later.

1.2 Nonsaturable losses

A high modulation depth of a SESAM is typically combined with nonsaturable material losses of the absorber. Additional losses are also caused by the bottom mirror, which supports the SESAM. Nonsaturable losses are not desired, because they only reduce the efficiency of the laser. A soft aperture in KLM introduces no losses at all, because only the gain is modulated. In contrast to the soft aperture, a hard aperture can introduce real losses, because the aperture has to cut the beam to obtain an efficient change in transmission between pulsed and cw operation. However, it is difficult to estimate how much the hard aperture finally contributes to nonsaturable losses.

1.3 Saturation behavior

To minimize the losses, the absorber should be saturable with the expected pulse fluence in the case of a slow absorber or with the pulse peak intensity in the case of a fast absorber. A quantitative criterion for a slow absorber is that the pulse energy in the laser should be several times more than the

saturation energy. If the pulse energy is far above the saturation energy, the laser tends to have multiple pulsing as observed in different laser systems [38, 54]. Therefore, the ideal saturation energy should be adaptable to the pulse energies expected or desired in the laser. It is difficult to define a saturation fluence in KLM lasers and even more difficult to measure it. However, the onset of multiple pulsing as observed in KLM Ti:sapphire lasers [54] gives a rough estimate of the present saturation fluence for a given laser set-up. In contrast, in soliton-modelocked lasers the saturation fluence of the SESAM can be determined by independent measurements [55, 56]. In the laser set-up, the incident pulse intensity onto the SESAM can then be adjusted by changing the incident mode area, i.e. by varying the focus, or by different SESAM designs [13]. Therefore, the saturation or of how many times the incident pulse energy fluence is above the saturation fluence can be adapted by using SESAMs.

1.4 Absorber recovery time

Another important parameter of the saturable absorber is its temporal response to an excitation pulse. It determines the maximum pulse shortening, i.e. the minimum achievable pulse duration, and the modelocking build-up characteristics of the laser. In a fast-saturable-absorber model, the recovery time of the saturable absorber is fast compared to the pulsewidth. Therefore, the open net-gain window is formed by the pulse itself and is as broad as the pulsewidth (Fig. 1a). In this way, the laser system discriminates against noise, which may grow outside the net-gain window. Thus, an ultrashort pulse is ideally kept stable by a fast saturable absorber. The artificial fast saturable absorber in KLM is as fast as the Kerr nonlinearity, which is estimated to be of the order of a few femtoseconds [57]. Hence, KLM is responsible for the shortest pulses obtained from Ti:sapphire lasers [10, 25, 29] and should be capable of supporting even shorter pulses if only the time response of the absorber is considered.

In the soliton-modelocking regime, we have shown that a slow saturable absorber can also support ultrashort pulses. If strong soliton formation is present, the pulsewidth can be much shorter than the absorber recovery time. The shortest pulsewidth we have obtained so far with pure soliton modelocking is 13 fs, using an absorber with a recovery time of only 60 fs (Fig. 5c). Figure 1b shows the computer simulation of the resulting absorber dynamics, the calculated gain level and the pulse intensity versus time. The saturable loss shown in Fig. 1b consists of the frequency-independent loss of the saturable absorber and the output coupler. It does not contain the losses introduced by the gain filtering and other spectral filtering elements in the laser cavity, which play a dominant role at the pulse durations considered. The open net-gain window is larger than the pulsewidth. One expects that this temporal behavior has consequences on the pulse quality, i.e., the presence of pulse pedestals growing in the open net-gain window. From this simple picture we would expect larger pulse pedestals for the soliton-modelocked pulses. However, we find similar pulse pedestals in both KLM pulses and soliton-modelocked pulses, by measuring their high-dynamic-range (HDR) autocorrelation [58]. Thus, soliton modelocking has the potential for generating even shorter pulses if the absorber is further optimized [20].

A fast saturable absorber is preferable for pulse shortening, but it only weakly supports the self-starting of sub-10-fs pulses as can be derived from Eq. (8) of [53]. There, the case of a homogeneously broadened laser is considered. Without any intracavity absorber, only one longitudinal cavity mode at the center of the gain is running. The gain is saturated, so that all neighbouring modes are below threshold. The saturable absorber causes two-mode coupling between the cavity mode at line center and the cavity mode m times the mode spacing $2\pi/T_R$ away from the line center. This two-mode coupling provides additional gain for the adjacent modes to reach threshold. The growth rate of these modes can be used as an estimate for the modelocking build-up time T_{MBT}. Note that we assume that the growing modes become phaselocked automatically and form a pulse. This may not always be the case and has been considered in [59]. For an absorber recovery time τ_A that is short compared to the roundtrip time T_R and a long normalized upper-state lifetime $T_L = \tau_L/T_R$ of the gain much greater than T_R, Eq. (8) of [53] can be simplified to the approximate condition

$$\frac{1}{T_{MBT}} \approx \left(\frac{2q_0}{E_A}\tau_A - \frac{2g_0}{(2m\pi)^2 T_L^2 P_L} \right) P \,, \tag{2}$$

where P is the intracavity laser power, $2q_0$ the modulation depth of the saturable absorber, $E_A = AE_{sat}$ is the saturation energy of the saturable absorber with E_{sat} the saturation fluence and A the incident laser mode area, g_0 is the small-signal amplitude gain coefficient, and P_L is the saturation power of the laser gain. As expected, the modelocking build-up time decreases with increasing intracavity power. The second term in (2) inside the brackets determines the threshold for self-starting as given by the laser parameters, which is independent of the intracavity power only in this simplified equation. The first term shows that a small saturation energy and a long absorber recovery time support the self-starting of modelocking. Therefore, the fast response of the artificial absorption due to KLM is detrimental for self-starting. Self-starting KLM lasers in the 10-fs pulse regime have not yet been demonstrated without any additional starting mechanisms such as feedback-initiated starting [29, 60] or a SESAM [30]. A clear advantage of using SESAMs is a simple and reliable starting of the modelocking process. Semiconductor absorbers typically show bitemporal behavior. The pump–probe measurement of broadband SESAM used in the soliton-modelocked 13-fs experiment shows not only the typical 60-fs time constant resulting from intraband thermalization [61], but also a long time constant in the picosecond regime resulting from carrier trapping and recombination (Fig. 5c). We benefit from this long time constant according to (2) because it is responsible for the self-starting.

1.5 Wavelength dependence

It should be mentioned that all absorber parameters discussed so far are ideally independent of the excitation wavelength. Otherwise, they would introduce an additional filter action resulting in a reduced net-gain bandwidth, which is detrimental for ultrashort-pulse generation. In principle, the Kerr nonlinearity is wavelength independent. However, a frequency-dependent mode size can cause some spectral limitations even

Table 2. Pulsewidths τ_p and modelocking build-up time T_{MBT} obtained with four different SESAMs in Ti:sapphire lasers

		KLM-assisted		soliton modelocking		Ref
	$2q_0$	τ_p	T_{MBT}	τ_p	T_{MBT}	
On semiconductor Bragg mirror						
- high-finesse A-FPSA	< 1%	19 fs		> 40 fs		[66]
- AR-coated thin absorber	5%			34 fs	3 μs	[67]
On silver mirror						
- low-finesse A-FPSA	1%	6.5 fs	3 ms	> 40 fs		[10]
- AR-coated thin absorber	5–6 %			13 fs	200 μs	[20]

in KLM [62]. But in the 6.5-fs experiments we could not find a direct proof for spectral limitation caused by KLM. This issue will become more critical with the generation of even shorter pulses.

The question of wavelength dependence can be clearly answered in the case of a SESAM. Semiconductors show wavelength-dependent absorption resulting in a wavelength-dependent modulation depth, nonsaturable loss, and saturation fluence. In general, the wavelength dependence is currently one of the major challenges in using SESAMs for sub-10-fs pulses. This issue is addressed in Sect. 2 and possible solutions are presented.

1.6 Spatio-temporal coupling and cavity design

The freedom to adjust absorber parameters means that the absorber should not be coupled to other pulse-shaping processes in the laser cavity. The soliton pulse-shaping in Ti:sapphire lasers is determined by the interplay of SPM and GDD. Therefore, the absorber parameters can be adjusted independently only if the absorber is not coupled to SPM or GDD in the laser cavity. Calculations show that the GDD of the SESAMs can be neglected. However, we observe a fundamental coupling of SPM to the saturable absorption in the case of KLM because SPM and the artificial saturable absorption created by the self-focusing in KLM depend on the mode size. This intensity-dependent self-focusing effect is even enhanced with KLM because the laser cavity is usually operated close to the stability limit, so that the cavity is sensitive to small intracavity lensing effects [63, 64]. Thus, KLM interrelates the laser mode size with the laser dynamics, leading to a complex spatio-temporal laser dynamics [65]. This results in a limited parameter range, thereby, restricting the cavity design. There are no such restrictions in the cavity design and parameter choice in a soliton-modelocked laser. For simplicity we typically use an additional focusing mirror to adjust the intensity on the SESAM. In principle we can design a SESAM with a specific saturation fluence by choosing different top reflectors in the case of an antiresonant Fabry–Perot saturable absorber (A-FPSA) [13, 23] or by placing the thin absorber layer at different positions within the SESAM [13]. There is no coupling between the saturable absorption and SPM as is the case in KLM.

Currently, the shortest self-starting pulses achieved directly out of a laser result from the combination of KLM with a SESAM as a starting mechanism. Figure 1c shows schematically the resulting absorber response in the 6.5-fs pulse experiments. We do not know the modulation depth of the fast contribution due to KLM, but the total time response consists now of three time constants. We use the advantages of soft-aperture KLM, the fast time response, the large modulation depth, and no nonsaturable losses, and combine them with the bitemporal behavior of a low-loss SESAM to start the pulses and to relax the critical cavity alignment. In the future we will optimize the modulation depth, the wavelengths dependence, and the time response of the SESAM in order to generate sub-10-fs soliton-modelocked pulses without the need for additional KLM. Once we have reached this goal we will be able to independently control the saturable absorption without being affected by SPM in the ultrashort pulse generation. This will be an important prerequisite for much higher average output power of sub-10-fs Ti:sapphire lasers, for example.

2 Semiconductor saturable absorbers for Ti:sapphire lasers

As discussed in Sect. 1, soliton modelocking with SESAMs has the potential to generate pulses much shorter than the fastest recovery time of the absorber. The realization of this goal depends strongly on the SESAM design. The SESAMs offer a distinct range of operating parameters, which have to be adjusted following the design criteria in Sect. 1. They should have a high modulation depth, a suitable saturation energy, a fast thermalization time constant for ultrashort-pulse generation, and a long time constant to start modelocking. In addition, bandwidth-limiting effects have to be minimized.

2.1 SESAM with an AlGaAs/AlAs *Bragg mirror*

The history of SESAMs used in Ti:sapphire lasers was determined by the design criteria for ultrashort-pulse generation (Fig. 2 and Table 2). The first SESAM for Ti:sapphire lasers was a high-finesse antiresonant Fabry–Perot saturable absorber (A-FPSA) based on the original intracavity saturable-absorber design [13, 23]. It consists of a lower semiconductor Bragg mirror and a dielectric top reflector, with a saturable absorber in between, as shown in Fig. 2a. The top reflector determines the amount of light that can penetrate and bleach the absorber. Therefore, the top reflectivity determines also the saturation fluence and the modulation depth. The top reflectivity was chosen to be relatively high to reduce the undesirable effects of the semiconductor of the bottom mirror such as losses and bandwidth limitation. With this design we produced 19-fs KLM-assisted pulses and 40-fs to 90-fs pulses in the soliton-modelocking regime [66]. However, the low modulation depth of less than 1% limited further pulse shortening of the soliton-modelocked pulses.

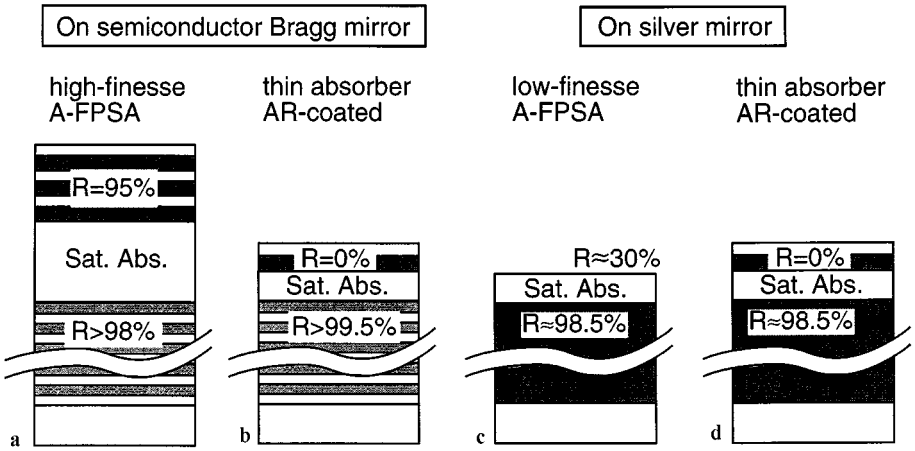

Fig. 2. Schematic overview of different SESAM devices used in Ti:sapphire lasers

A higher modulation depth was achieved with another SESAM design where the top reflector was replaced by an antireflection (AR-) coating (Fig. 2b) [67]. In this case, the thickness of the absorber structure had to be reduced to minimize insertion losses. The total structure on top of the semiconductor Bragg mirror consists of 50-nm AlAs as a transparent spacer layer, a 15-nm LT-GaAs quantum well, and an Al_2O_3 AR coating as shown in Fig. 3a. A modulation depth of 4.9% and a saturation fluence of 18 $\mu J/cm^2$ have been evaluated from independent saturation measurements (Fig. 3b). This increased modulation depth resulted in self-starting 34-fs pulses obtained over the full cavity stability regime. Furthermore, a modelocking build-up time of only $\approx 3\,\mu s$ was measured [66, 67]. In this experiment the modelocking mechanism is not based on fast saturable-absorber modelocking but on soliton modelocking, because the measured impulse response shows a fast time constant of only 100 fs and a longer one of 6 ps due to trapping and recombination (Fig. 3c). The high modulation depth could have supported even shorter pulses, but the reflection bandwidth of the lower AlGaAs/AlAs Bragg mirror limited further pulsewidth reduction. Note that we obtained shorter pulses of 19 fs with the high-finesse A-FPSA by using the same lower AlGaAs/GaAs Bragg mirror. However, an AR-coating instead of a relatively high reflecting top reflector with a larger reflection bandwidth exposes the strong bandwidth limitation of the lower Bragg mirror. The bandwidth is fundamentally limited by the small differences in the refractive indices of AlGaAs and GaAs.

2.2 Broadband SESAM with a silver mirror

A solution to the bandwidth limitation of an AlGaAs/AlAs Bragg mirror was to replace the semiconductor Bragg mirror by a silver mirror [30]. The silver mirror provides a reflectivity of more than 98% from about 500 nm to the far-infrared region. First, we used such a silver mirror in a low-finesse A-FPSA design [13, 39, 66]. It is called low finesse, because the top reflector is now formed by the semiconductor–air interface, resulting in about 30% top reflection (Fig. 2c). To preserve the large bandwidth of the silver mirror, we used a thin absorber structure with a large free spectral range. In addition, we reduced the wavelength dependence of the absorption edge of GaAs by low-temperature MBE growth and by using transparent spacer layers that shift the absorber layer to a specific position in the wavelength-dependent standing-wave pattern (Fig. 4a). Using this broadband SESAM, we obtained self-starting, KLM-assisted 10-fs pulses [30]. Recently, we obtained self-starting KLM-assisted 6.5-fs pulses after improved dispersion compensation (see Sect. 3 and Fig. 9) [10]. In this case we measured a modelocking build-up time of about 3 ms. With the simple low-finesse A-FPSA design (Fig. 4a) we obtained a broadband SESAM with minimal wavelength dependence but at the expense of the modulation depth of $\approx 1\%$ (Fig. 4b), which was not large enough to stabilize pure soliton modelocking. Actually, the modulation depth of the fast ≈ 50-fs component required to support sub-10-fs pulses with soliton modelocking is only about 20% of the maximum modulation (Fig. 4c). Thus, the sub-10-fs pulses needed the assistance of a fast saturable absorber such as KLM. However, the broadband SESAM provided self-starting modelocking because of the slow 12-ps recovery time (Fig. 4c) and somewhat relaxed the critical cavity alignment for KLM. Note that the saturation measurements performed with 100-fs and 13-fs excitation pulses (Fig. 4b) resulted in approximately the same modulation depth ΔR and nonsaturable losses ΔR_{ns}. However, we observe a larger saturation fluence E_{sat} for shorter pulses, which is not surprising and will be discussed later in this section.

With another broadband SESAM using more GaAs absorber layers and an AR coating (Fig. 5a) we increased the modulation depth to $\approx 6\%$, which we extracted from saturation measurements by using 13-fs excitation pulses (Fig. 5b). As for the SESAM before, we observed a bitemporal impulse response (Fig. 5c) with a fast component of 60 fs (intraband thermalization [61]) and a slow component of ≈ 700 fs (carrier trapping and recombination). The post-growth processing required for the silver mirror is probably responsible for the relatively fast sub-picosecond trapping and recombination time. This is not desirable because it increases the modelocking build-up time, as will be discussed in the next section. With this SESAM we generated soliton-modelocked 13-fs pulses over the full cavity stability range with a modelocking build-up time of 200 μs (Fig. 5d) [20]. No KLM assistance was required.

Figure 5b shows the saturation of the SESAM for a 100-fs and a 13-fs excitation pulse. However, we did not determine the pulsewidth incident on the SESAM inside the laser cavity. We would expect a longer pulse duration than 6.5 fs because

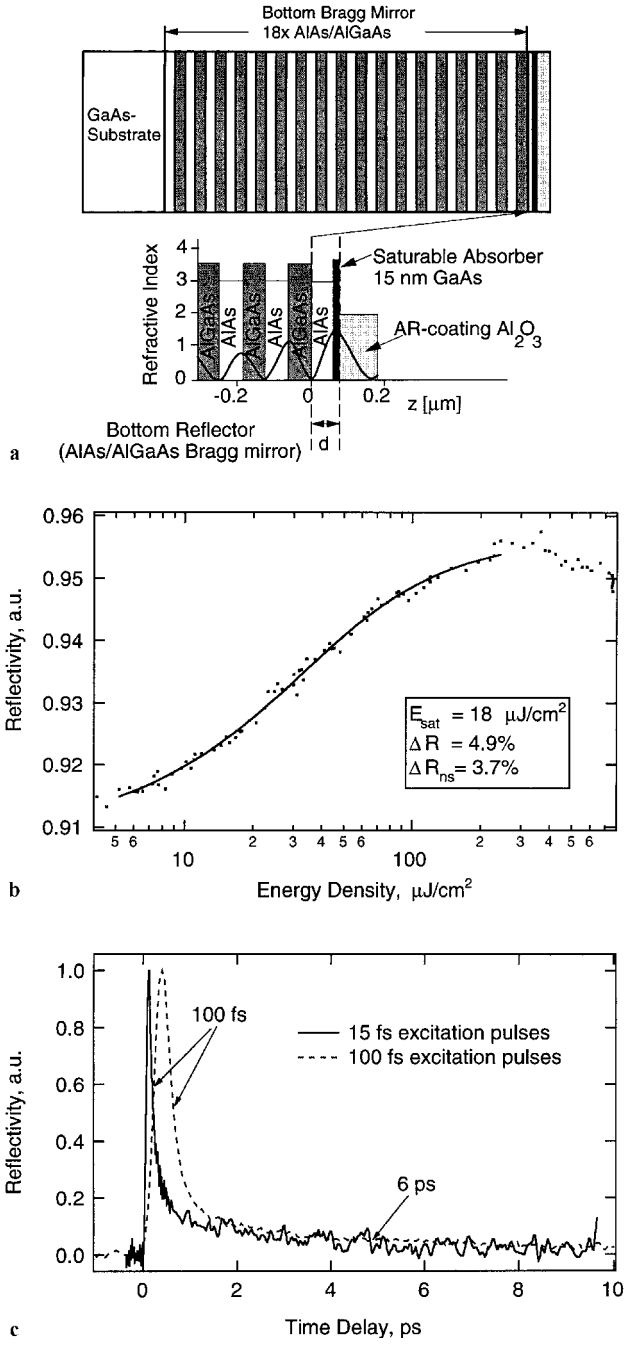

Fig. 3. a AR-coated SESAM with a AlGaAs/AlAs bottom mirror which starts and stabilizes 34-fs pulses with soliton modelocking and a modelocking build-up time of $\approx 3\,\mu$s. **b** Saturation measurement with 100-fs pulses at 830 nm. A theoretical fit using traveling-wave rate equations (Eqs. 17 and 18 in [56]) gives a saturation fluence of $18\,\mu J/cm^2$, a maximum modulation depth ΔR of 4.9%, and a nonsaturable loss ΔR_{ns} of 3.7%. **c** Degenerate noncollinear pump–probe measurement at a center wavelength of 830 nm with 100-fs and 15-fs excitation pulses with perpendicular and parallel polarization, respectively. The bitemporal impulse response shows a fast time constant of 100 fs and a slow time constant of 6 ps. The excitation level was around 6 times the saturation fluence of the device

the pulsewidth inside the laser cavity changes drastically because of the discrete elements with either positive or negative dispersion [25]. Therefore, we compare the modulation depth obtained from the saturation measurements with the following estimation obtained directly from the starting dynamics of the modelocked laser (Fig. 5d). The second-harmonic signal of the output power generated in a nonlinear crystal scales inversely with the pulse duration and therefore indicates the onset of modelocking. As seen from Fig. 5d, the average output power increases by a factor of 2 between cw and pulsed operation. Assuming a homogeneously broadened laser gain medium, we can estimate the actual modulation depth of the SESAM inside the laser using the condition [68] $g = l = g_0(1+2P/P_L)^{-1}$, where g represents the saturated amplitude gain coefficient at cw or pulsed operation (i.e. g_{cw} or g_p), l represents the total amplitude loss coefficient at cw or pulsed operation (i.e. l_{cw} or l_p), g_0 represents the small-signal amplitude gain coefficient at cw or pulsed operation (i.e. $g_{0,cw}$ or $g_{0,p}$), P represents the average intracavity power inside the laser at cw or pulsed operation (i.e. P_{cw} or P_p), and P_L is the saturation intensity of the laser medium. We determine $2l_{cw} \approx 0.16$ from the fact that the total intracavity loss at cw is $\approx 16\%$ as a result of the 3% output coupler, the measured modulation depth of 6%, and the nonsaturable losses of about 7% (Fig. 5b). The nonsaturable losses vary slightly depending on the spot position on the SESAM. Since the laser is optimized for maximum output power, we have chosen the smallest value of the nonsaturable losses we obtained in the saturation measurements. In addition, $g_{0,cw} \approx 3l_{cw}$ because at cw operation the laser is pumped ≈ 3 times above threshold. With $2l_{cw} \approx 2l_p + \Delta R$ and $P_p \approx 2P_{cw}$ (from Fig. 5d) we then determine a modulation depth $\Delta R \approx 6.4\%$, which is consistent with the saturation measurement shown in Fig. 5b.

2.3 Broadband SESAM with an AlGaAs/*fluoride Bragg mirror*

Another approach used to obtain a broadband SESAM for sub-10-fs pulse generation is based on AlGaAs/fluoride Bragg mirrors, which provide a large spectral bandwidth because of the large difference in the refractive indices of the fluorides and AlGaAs [69, 70]. Figure 6 shows the measured wavelength-dependent reflectivity of such a fluoride Bragg mirror, designed for a center wavelength of 750 nm, consisting of 4 pairs of $Al_{0.78}Ga_{0.22}As$ and CaF_2. They provide more than twice as much spectral bandwidth compared to the original semiconductor Bragg mirrors consisting of $Al_{0.15}Ga_{0.85}As$ and AlAs. The maximum reflectivity is 98.5%, which is similar to that of a silver mirror. However, in contrast to the case of a silver mirror, the absorber structure can be directly grown on the fluoride Bragg mirror. No damage or degradation was observed in preliminary experiments, in which the SESAM on a silver mirror was replaced by such a fluoride mirror. With such a SESAM device we expect better high-power performance in the future.

2.4 Modelocking build-up time

With (2) we can explain the modelocking build-up time we observed with the different SESAMs discussed before. We define the first term in (2) as the saturable absorption coefficient γ, because it describes the slope of a fast saturable absorption $2q = 2q_0(1+P/P_A)^{-1}$ at zero intensity, where the saturation power is $p_A = E_A/\tau_A$, given a certain mode size on

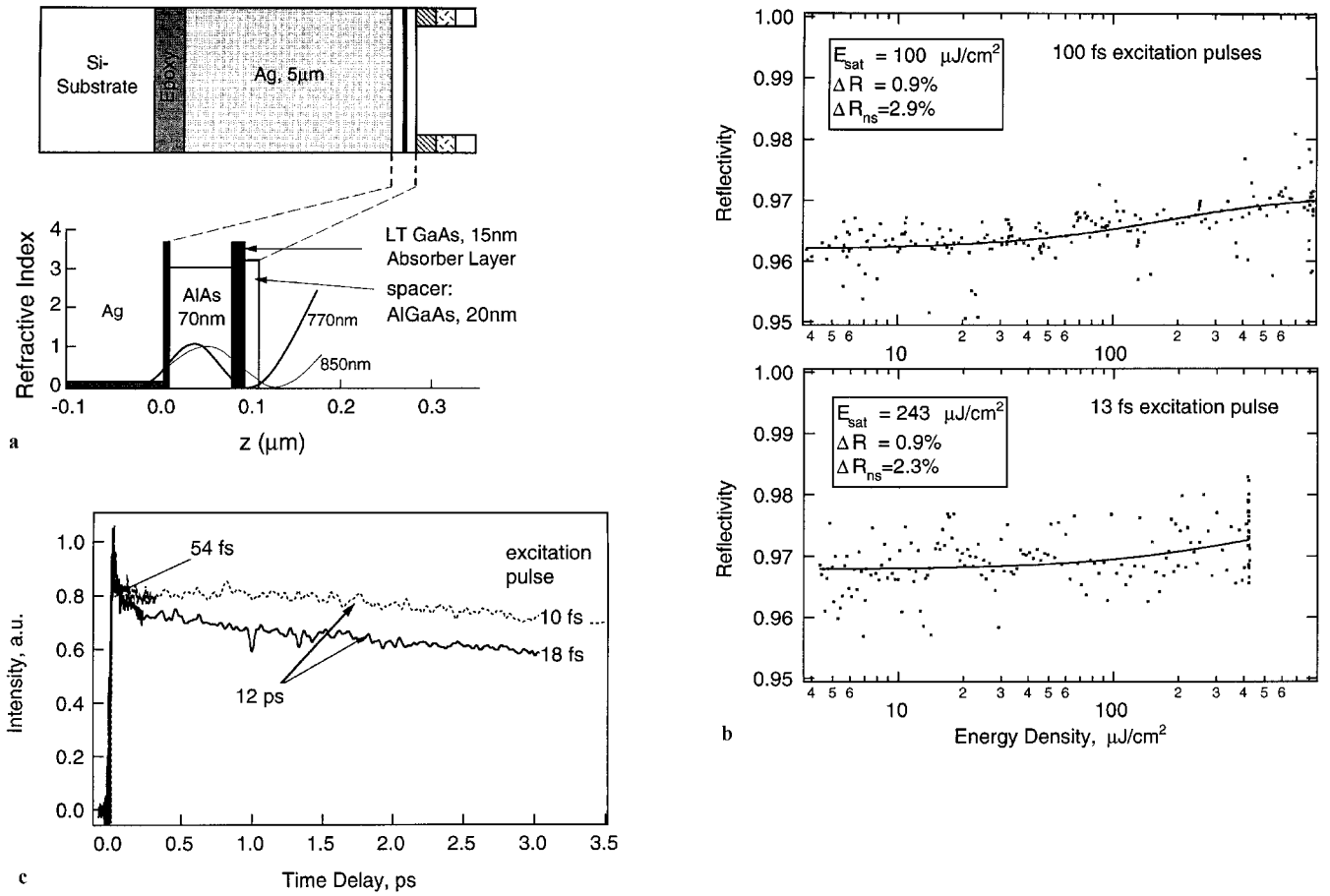

Fig. 4. a Broadband SESAM based on a low-finesse A-FPSA design that starts 6.5-fs KLM pulses with a modelocking build-up time of ≈ 3 ms. The calculated standing-wave intensity distributions for $\lambda = 770$ nm and 850 nm show the location of the 15-nm thick GaAs absorber layer in the standing-wave pattern. At shorter wavelengths we obtain a lower incident intensity, which counteracts the wavelength dependence of the GaAs absorption edge. **b** Saturation measurements with ≈ 100-fs pulses at 800 nm and with ≈ 13-fs pulses at 795 nm. A theoretical fit using traveling-wave rate equations (Eqs. 17 and 18 in [56]) gives a saturation fluence of 102 μJ/cm^2 and 243 μJ/cm^2, respectively, a maximum modulation depth ΔR of 0.9%, and nonsaturable losses ΔR_{ns} of 2.9% and 2.3%, respectively. **c** Degenerate noncollinear pump–probe measurements at a center wavelength of 800 nm with 10-fs and 18-fs excitation pulses with parallel polarization. The bitemporal impulse response shows a fast time constant of 54 fs and a slow time constant of 12 ps. The incident pulse energy density is ≈ 40 μJ/cm^2

the absorber, and the incident laser power:

$$\left|\frac{\mathrm{d}(2q)}{\mathrm{d}I}\right|_{I=0} = \gamma = \frac{2q_0}{E_{\mathrm{A}}}\tau_{\mathrm{A}}\,. \tag{3}$$

Using typical values for our passively modelocked Ti:sapphire laser, a saturation power of the laser gain $P_{\mathrm{L}} = 4$ W, a small-signal gain amplitude coefficient $g_0 \approx 0.2$, and a normalized upper-state lifetime $T_{\mathrm{L}} = 3\,\mu\mathrm{s}/10\,\mathrm{ns} = 300$, we obtain from (2) a threshold value for γ needed to achieve self-starting of modelocking:

$$\gamma > 2.8 \times 10^{-8}\frac{1}{\mathrm{W}}\,. \tag{4}$$

Here, we assumed that the next neighbouring mode has to couple to the mode at line center to initiate the modelocking, i.e. $m = 1$.

Using the SESAM shown in Fig. 3, we determine with (3) a saturable absorption coefficient of $\gamma = 1.5 \times 10^{-4}$ 1/W. This results in a modelocking build-up time of about 13 μs. We used the following measured parameters: $2q_0 \approx \Delta R \approx 0.05$ (Fig. 3c), $P = 5$ W, $\tau_{\mathrm{A}} = 6$ ps (Fig. 3c), and $E_{\mathrm{A}} = AE_{\mathrm{sat}} = 2$ nJ, assuming a saturation fluence $E_{\mathrm{sat}} = 18$ μJ/cm^2 (Fig. 3b) and a focused laser-mode radius of 60 μm on the SESAM (estimated from ABCD matrix calculations). The threshold condition is clearly fulfilled and the calculated value of the modelocking build-up time is on the order of the experimental value of 3 μs.

Using the SESAM shown in Fig. 5 we observed a slow recovery time of only $\tau_{\mathrm{A}} = 730$ fs (Fig. 5c), which is most likely to be because of the post-growth processing. Therefore, we calculate with (3) that $\gamma = 3.2 \times 10^{-5}\,\mathrm{W}^{-1}$ and with (2) a modelocking build-up time of 137 μs, using $2q_0 \approx \Delta R \approx 0.052$ (Fig. 5b), $P = 5$ W, and $E_{\mathrm{A}} = AE_{\mathrm{sat}} = 1.2$ nJ and assuming a saturation fluence $E_{\mathrm{sat}} = 40$ μJ/cm^2 (Fig. 5b) and a focused laser mode radius of 30 μm on the SESAM (estimated from ABCD matrix calculations). For the modelocking build-up time we use the saturation fluence of the longer 100-fs excitation pulse. This is justified because during most of the modelocking build-up phase shown in Fig. 5d the second-harmonic signal is very small, which implies that the pulse duration is rather long. The simple theoretical prediction of 137 μs is again in good agreement with the measured value of 200 μs.

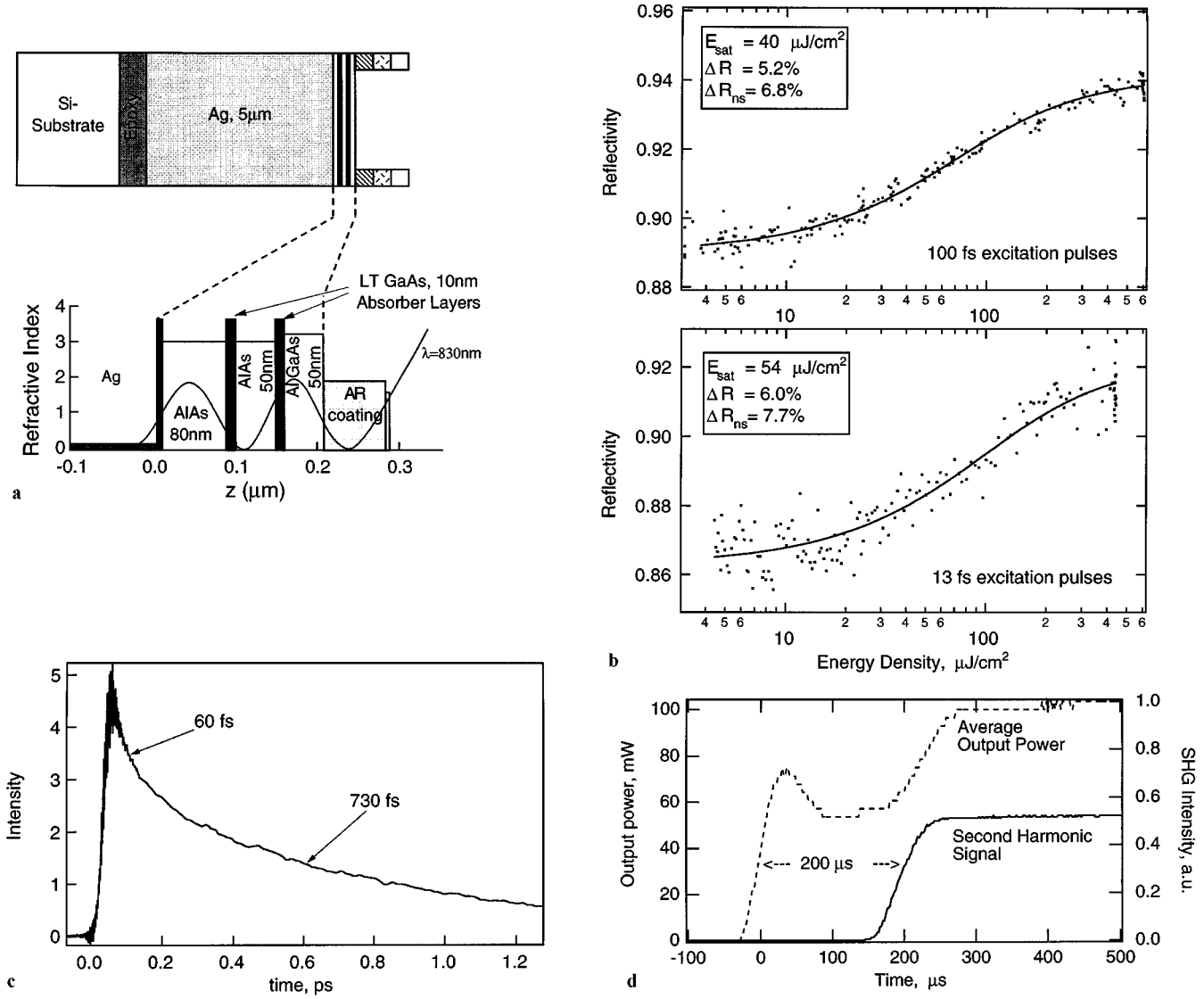

Fig. 5. a AR-coated SESAM design which starts and stabilizes 13-fs pulses with soliton modelocking and a modelocking build-up time of 200 μs. The location of the two 10-nm-thick GaAs absorber layers with respect to the standing-wave pattern is shown. **b** Saturation measurement with ≈ 100 fs pulses at 825 nm and with ≈ 13 fs at 795 nm. A theoretical fit using traveling-wave rate equations (Eqs. 17 and 18 in [56]) gives a saturation fluence of 40 μJ/cm^2 and 54 μJ/cm^2, a maximum modulation depth ΔR of 5.2% and 6%, and nonsaturable losses ΔR_{ns} of 6.8% and 7.7%, respectively. **c** Degenerate noncollinear pump–probe measurement at a center wavelength of 810 nm with 10-fs excitation pulses with parallel polarization. The bitemporal impulse response shows a fast time constant of 60 fs and a slow time constant of 730 fs. The incident pulse energy density is ≈ 65 μJ/cm^2 at about 1.2 times the saturation fluence of the device. **d** Modelocking build-up time of 200 μs measured with an intracavity chopper. The dynamical behavior of the average output power gives an estimate for the modulation depth of ≈ 6.4% for the SESAM inside the Ti:sapphire laser generating 13-fs pulses

Thus, we can still achieve the threshold for self-starting modelocking, but the much smaller absorber recovery time leads to a drastic increase in the modelocking build-up time.

It is instructive to have a closer look at the parameters of a purely KLM system. If we assume a modulation depth of $2q_0 = 0.2$, an intracavity laser power of 6.7 W, an absorber response time of 2 fs, and a saturation energy of 5–20 nJ, we obtain for the saturable absorption coefficient $\gamma = 2 \times 10^{-8}$ to 8×10^{-8} W^{-1} (from (3)), which is very close to the threshold value (from (4)). This very rough estimation shows that KLM pulses in the 10-fs regime typically do not self-start, because of the fast response time. Self-starting pulses with pulse durations of 50 fs and more have been demonstrated by optimizing KLM [71, 72]. However, a modelocking build-up time of several milliseconds with strong statistical fluctuations has been measured [71]. From our calculations we observe that the modelocking build-up time of KLM is in the range of milliseconds and higher. In the 6.5-fs experiment, KLM had to be optimized to obtain self-starting pulses, but self-starting was never observed without the SESAM.

2.5 Wavelength dependence

The results we obtained with the different SESAM designs, shown in Figs. 3 to 5, clearly demonstrate the challenge in reducing the wavelength dependence of the absorption in semiconductors. We have demonstrated that we can reduce the wavelength dependence with thin absorber layers at specific positions with respect to the standing-wave pattern (Fig. 4a

and Fig. 5a). At shorter wavelengths we have a limitation due to intervalley scattering between the Γ and the L valley in GaAs. The difference between the minimum energies of the valley and the valley is 0.31 eV in bulk GaAs [73]. Spectral components of the pulse spectrum with a wavelength shorter than 715 nm generate carriers that rapidly scatter into the L valley. Therefore, the absorption can no longer be bleached, which introduces an additional wavelength filter. As a consequence, the center part of a sub-10-fs pulse centered at 780 nm may saturate the semiconductor, but the low-intensity tail at shorter wavelengths will be absorbed. This is the reason why we could not tune the 13-fs pulses to a center wavelength shorter than 770 nm without significant pulse broadening or pulse break-up by using the broadband SESAM shown in Fig. 5 and soliton modelocking.

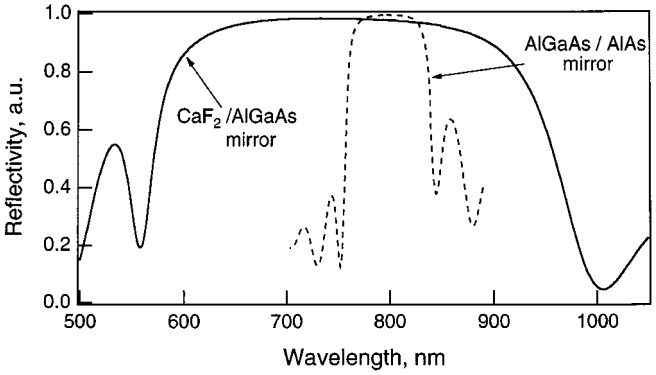

Fig. 6. Measured reflectivity of an AlGaAs/fluoride Bragg mirror with four pairs of $Al_{0.78}Ga_{0.22}As$ and CaF_2 in comparison to a standard $AlAs/Al_{0.15}Ga_{0.85}As$ Bragg mirror with 25 pairs

2.6 Pulsewidth dependence

The population decay in semiconductor materials shows a typical bitemporal time response consisting of a slow and a fast time constant. The slow time constant τ_c is in the range of ps to ns as a result of carrier trapping or recombination and the fast time constant τ_{th} is in the range of a few tens of femtoseconds because of intraband thermalization. At high excitation densities, the carriers thermalize amongst each other because of carrier–carrier scattering to form a hot Fermi–Dirac distribution [74]. For high carrier densities the

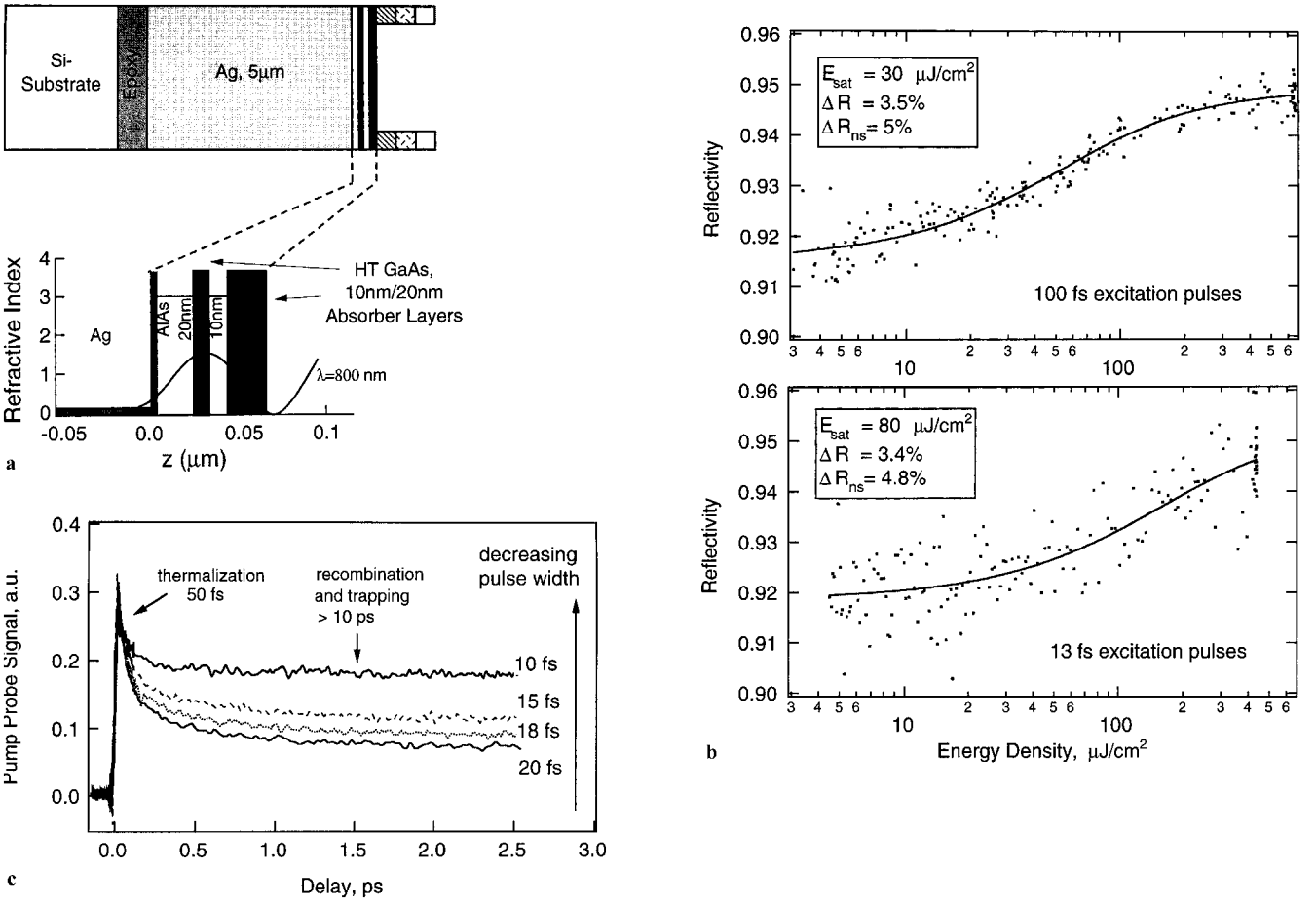

Fig. 7. a Broadband SESAM, which supported 10–15 fs pulses with additional KLM assistance and pulses as short as 20 fs with soliton modelocking. **b** Saturation measurement with ≈ 100 fs pulses at 805 nm and with ≈ 13 fs at 795 nm. A theoretical fit using traveling-wave rate equations (Eqs. 17 and 18 in [56]) gives a saturation fluence of 30 $\mu J/cm^2$ and 80 $\mu J/cm^2$, a maximum modulation depth ΔR of 3.5% and 3.4%, and nonsaturable losses ΔR_{ns} of 5% and 4.8%, respectively. **c** Degenerate noncollinear pump–probe measurement with parallel polarization at a center wavelength of 800 nm with 10-fs to 20-fs pulse duration at an incident pulse energy density of ≈ 250 $\mu J/cm^2$. The contribution from the thermalization time constant decreases with decreasing pulsewidth

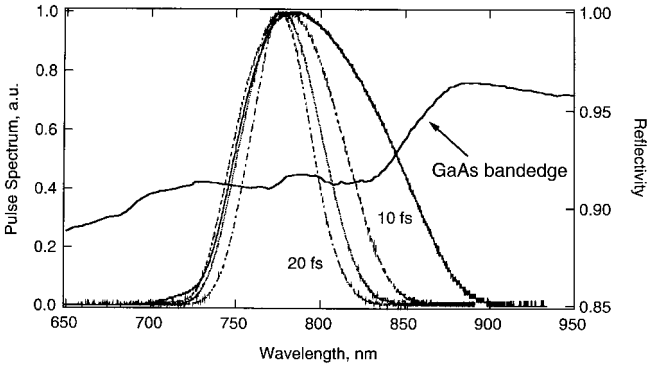

Fig. 8. Pulse spectra of the excitation pulses used in the pump–probe measurements of Fig. 7c in comparison with the low-intensity reflectivity of the broadband SESAM of Fig. 7a. The step is caused by the bandedge of GaAs

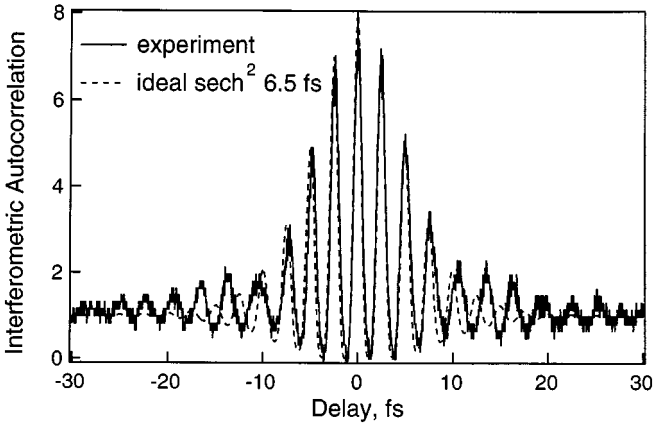

Fig. 9. Interferometric autocorrelation of a self-starting 6.5-fs pulse, achieved directly from the laser, in comparison with an ideal 6.5-fs sech^2 pulse at 750 nm

thermalization time in bulk GaAs is ≈ 60 fs [61]. Therefore, the fast-thermalization time constant of the SESAMs is the slow recovery time τ_A associated with the ultrashort-pulse generation with soliton modelocking. Thus, the modulation depth corresponding to this recovery time should be as high as possible. However, the modulation depth due to the thermalization process depends on the excitation-pulse duration (Fig. 4c and Fig. 7c) and decreases with shorter pulses. Unfortunately, the decrease in the modulation depth of the fast component counteracts further pulse shortening. This has to be compensated for by an additional fast saturable absorber such as KLM.

The pulsewidth dependence of the modulation depth of the fast contribution is shown in Fig. 7c for the SESAM shown in Fig. 7a. The incident pulse energy density of $\approx 250\,\mu J/cm^2$ was constant for all measurements and is about 8 times the saturation fluence of the device (Fig. 7b). This is a typical excitation level inside the laser. It was shown that the dephasing time decreases with increasing carrier density in bulk GaAs as well as in GaAs quantum wells [75, 76]. A dephasing time of ≈ 15 fs has been measured at a carrier density $N \approx 10^{11}\,cm^{-2}$ [76]. For our experiments, we estimate from the absorbed pulse energy a carrier density of about $4 \times 10^{13}\,cm^{-2}$. Assuming a density-dependent dephasing time that scales as $N^{-0.55}$ [76], we would expect a dephasing time of ≈ 6 fs. Therefore, as a first approximation for pulses longer than 10 fs, we can neglect coherent effects as a contribution to the pump probe measurements shown in Figs. 4c and 7c. However at this point, it is not clear if we can use this scaling law at carrier densities which are nearly two orders of magnitude higher. Further investigations are required and are in progress.

Assuming that coherent effects are negligible, we can give a qualitative explanation for the pulsewidth dependence in Fig. 7c. Figure 8 shows the spectra of the excitation pulses and the low-intensity reflectivity of the SESAM shown in Fig. 7a. A larger fraction of the conduction-band states are excited with broader spectrum. Carriers created by the 10-fs pulse are equally distributed from the band edge to energy levels corresponding to a wavelength of 740 nm. The resulting carrier distribution is closer to a hot quasi-equilibrium distribution than a distribution generated by a 20-fs pulse at 760 nm. Thus, carrier-carrier scattering that leads to a hot quasi-equilibrium distribution is reduced for the broadband excitation with the 10 fs pulse. Therefore, we can increase the fast modulation depth and reduce the undesired pulsewidth dependence when we excite high into the conduction band such that the thermalized carriers can leave the spectral region of the excitation pulse towards the conduction-band edge. However, in our current GaAs absorbers this is prohibited by intervalley scattering that occurs for higher excitation energies. Therefore, more sophisticated semiconductor bandgap engineering will be required for improved broadband SESAMs that could support pure soliton modelocking in the sub-10-fs regime.

From a purely phenomenological point of view, we must accept that an increased saturation fluence with shorter pulses can counteract further pulse shortening. This can be prevented only by operating the SESAM at an incident pulse energy density that fully saturates the absorber also in the final short-pulse regime, because the maximum modulation depth does not depend on the excitation pulse duration (Figs. 4, 5, and 7). However, an upper limit is set by the onset of multiple pulsing [38].

3 Sub-10-fs pulses started by broadband SESAMs

Currently, the shortest pulse produced directly from a laser is a self-starting, KLM-assisted (see Sect. 1) 6.5-fs pulse where a broadband, low-finesse SESAM (Fig. 4) is used as a starting mechanism [10]. The measured interferometric autocorrelation (IAC) trace is shown in Fig. 9. We have evaluated a pulse duration of 6.5 fs from the measured IAC trace by comparison with an ideal sech^2 pulse shape. We obtained these pulses with an average output power of 200 mW and a modelocking build-up time of about 3 ms. Another key point for this success is the improved dispersion compensation of the laser cavity obtained by using double-chirped mirrors [22] in combination with a prism pair. Prism pairs are well established for intracavity dispersion compensation [26] and offer two advantages. First, the pulsewidth can be varied by simply moving one of the prisms, and second, the laser can be tuned in wavelength by simply moving a knife edge at a position where the beam is spectrally broadened. Both properties are often desired for spectroscopic applications, for example. However, the prism pair suffers from higher-order dispersion, which is the main limitation in pulse shortening [25].

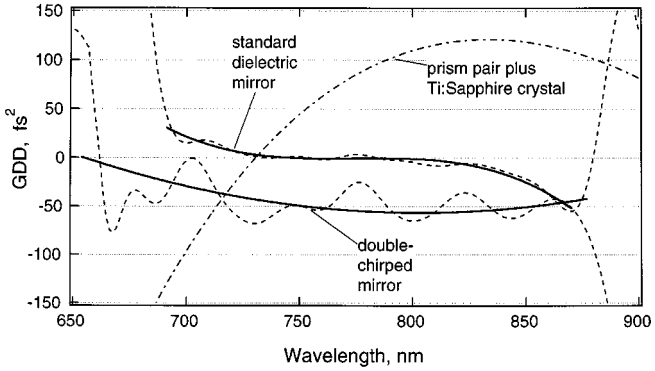

Fig. 10. Group delay dispersion (GDD) of the different optical elements in the laser cavity. (· — ·—) Calculated GDD of the prism pair and the Ti:sapphire crystal; (— — — —) measured GDD of the double-chirped mirror and of one Spectra Physics high reflector; (———) average GDD in both measurements

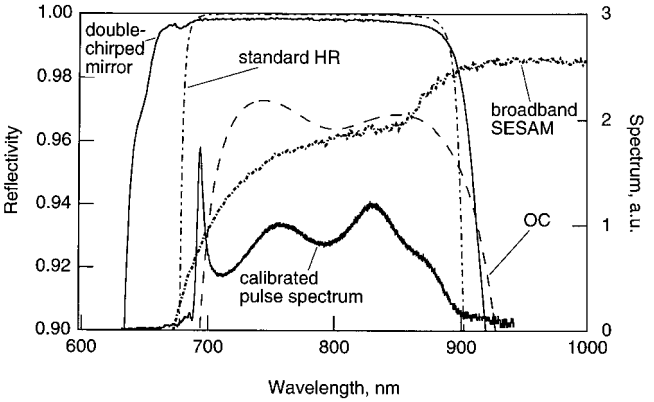

Fig. 11. Reflectivity of the broadband SESAM in Fig. 4, the output coupler (OC), the Spectra Physics high reflector (HR), the double-chirped mirror, and the pulse spectrum

Therefore, double-chirped mirrors were designed to show the inverse higher-order group delay dispersion of the GDD of the prism pair plus laser crystal to eliminate the higher-order dispersion.

Chirped multilayer structures for dispersion compensation in femtosecond laser systems have been introduced [21, 27, 28, 77] and are described in more detail by Szipöcs in this issue of *Applied Physics B*. Chirped mirrors overcome the bandwidth limitation and simultaneously provide a means for compensation of the group delay dispersion in the laser. However, so far the chirped mirror design is done by computer optimization [21], because a simple chirping of the center wavelength of the Bragg mirror is not enough [22, 78]. It would introduce oscillations in the group delay for longer wavelengths, which penetrate deeper into the mirror. The oscillations are due to an effective Gire–Tournois interferometer, created by partial reflection from the front section of the mirror, which acts as a transmission grating, and the reflection at the back of the mirror, which acts as a Bragg reflector.

We call our mirrors double-chirped mirrors after the following considerations. The chirp of a mirror can be understood as a continuous increase of the Bragg wavelength λ_B, which is twice the optical thickness of a layer pair. Such a pair consists of a layer with a low refractive index and one with a high refractive index, typically each with an optical thickness of $\lambda_B/4$. A simple chirp would be a continuous increase in the Bragg wavelength caused by continuously increasing both quarter-wave layers. In the double-chirped mirrors, we chirp not only the Bragg wavelength of the layer pairs, but separatly also the high-index layer in every pair according to a certain power law. The low-index layer in a pair is adapted so that the total optical thickness is approximately $\lambda_B/2$. A chirp of the high index layer corresponds to a chirp of the coupling coefficient, which is a measure of the coupling in the reflected wave [79]. In [22] we have shown that an impedance mismatch at the front of the mirror is responsible for the strong oscillations in the GDD. This mismatch can be avoided by adiabatically switching on the coupling coefficient.

The measured GDD due to one reflection on the double-chirped mirror and that on a standard dielectric mirror (Spectra Physics) are shown in Fig. 10. The bold lines correspond to average GDD. Furthermore, Fig. 10 shows the calculated GDD of the prism pair with 40 cm from prism to prism and a 6-mm total prism insertion in combination with the laser crystal per roundtrip. The contribution of the output coupler is less severe than the contribution from the standard high reflectors, and therefore it is not shown. The net GDD of the laser cavity (Fig. 2 in [10]) is given by the sum of all contributing GDD curves of each element. Within one cavity roundtrip, the pulse experiences six reflections from standard dielectric mirrors and two reflections from the double-chirped mirror. The double-chirped mirror improves the effective GDD in the laser cavity, because the average GDD of the double-chirped mirror was designed to show the inverse behavior of the GDD of the prism pair if three intracavity mirrors would have been used. Additionally, the fitted GDD of the double-chirped mirror slightly increases again at longer wavelengths, which counteracts both the reduced slope of the standard dielectric mirrors beyond 850 nm and the slowly decreasing GDD of the prism pair. Thus, the use of the double-chirped mirror results in a reduction of higher-order dispersion over a larger spectral range. However, the oscillations in the GDD, which are currently due to a limited number of layers in the double-chirped mirror design, cause a modulation in the pulse spectrum. This limited us to only two reflections from the double-chirped mirror. This will be improved in the near future.

Figure 11 shows the reflectivity of all intracavity elements and the pulse spectrum calibrated with respect to the wavelength-dependent sensitivity of the spectrometer. The pulse spectrum changes slightly depending on the position of the laser beam on the spectrometer slit. This indicates the presence of a frequency-dependent mode size, which is typical in sub-10-fs KLM lasers [62] and needs further investigations. Therefore, the acquisition of a correct broadband pulse spectrum has still some uncertainties. The pulse spectrum itself shows significant deviations from an ideal sech^2 shape. We think they are mainly caused by the oscillations in the GDD of the double-chirped mirror. However, the double-chirped mirror provides a broad spectral bandwidth from 650 nm to 900 nm with a reflectivity as large as 99.8%. The high optical quality of the double-chirped mirrors is due to the low-loss fabrication process with an ion beam sputtering technique [80, 81]. The available bandwidth

is clearly limited by the bandwidth of the remaining standard dielectric mirrors. Therefore, further improvements are expected when all mirrors in the laser cavity are replaced by double-chirped mirrors and the oscillations in the GDD are reduced by an increased number of dielectric layers in the mirror.

The pulsewidth resulting from the Fourier-transformed spectrum, assuming a constant phase over the full spectrum, is slightly longer than the 6.5 fs. However, considering the uncertainties in the measured spectrum as discussed above, the agreement is reasonable and we adopt the pulsewidth derived from the interferometric autocorrelation as has been done before [25, 29, 82].

4 Conclusion

During the last 5 years, the pulsewidth of pulses obtained directly from a Ti:sapphire laser has been reduced by a factor of five, reaching 6.5 fs. The significant success in achieving self-starting 6.5-fs pulses directly from a laser was possible only because of the development of broadband SESAMs and improved dispersion compensation.

The development of broadband SESAMs is an important contribution in achieving reliable self-starting sub-10-fs lasers with potentially no critical cavity alignments. So far, we have demonstrated self-starting, soliton-modelocked 13-fs pulses over the full cavity stability regime. The availability of shorter pulses obtained by pure soliton modelocking depends on further improvements of the broadband SESAM design. Optimization of the absorber requires a better understanding of the saturation behavior and the temporal response on a 10-fs time scale. In addition, adequate absorbers require more sophisticated bandgap engineering. There are possibilities to influence the band structure of the absorber in the SESAM by adding indium or changing to a new material system such as InP.

We have also demonstrated a broadband SESAM, which starts and supports KLM pulses of a Ti:sapphire laser. Using such a SESAM, we obtained self-starting 6.5-fs pulses with the assistance of KLM. The SESAM shows a flat reflectivity over more than 200 nm as a result of a balance between the wavelength dependences of the absorption in GaAs and the standing wave pattern. Since we used a quantum well with a low modulation depth for this SESAM, the wavelength dependence in the absorber properties is negligible. Owing to the low modulation depth, this SESAM also has fewer nonsaturable losses, resulting in an average output power of 200 mW.

Higher-order dispersion of the laser optics and the prism pairs, and the finite bandwidth of the laser optics are still the main limitations in further pulse shortening. The invention and development of chirped and double-chirped mirrors offers a solution to this problem. Our approach, the combination of prism pairs with double-chirped mirrors, has been essential in the generation of the shortest pulses obtained directly from a laser. Further improvements are expected in the near future with the replacement of all laser mirrors by an improved double-chirped mirror design.

We would like to acknowledge helpful discussions with Dr. Uwe Siegner. This work was supported by the Swiss National Science Foundation.

References

1. U. Keller: Current Opinion in Solid State & Materials Science **1**, 218 (1996)
2. M. Joschko, M. Woerner, T. Elsaesser, E. Binder, T. Kuhn, R. Hey, H. Kostial, K. Ploog: Phys. Rev. Lett. **78**, 737 (1997)
3. S. Backus, J. Peatross, Z. Zeek, A. Rundquist, G. Taft, M.M. Murnane, H.C. Kapteyn: Optics Lett. **21**, 665 (1996)
4. I.P. Christov, J. Zhou, J. Peatross, A. Rundquist, M.M. Murnane, H.C. Kapteyn: Phys. Rev. Lett. **77**, 1743 (1996)
5. J. Zhou, J. Peatross, M.M. Murnane, H.C. Kapteyn: Phys. Rev. Lett. **76**, 752 (1996)
6. A.M. Weiner: Prog. Quant. Electr. **19**, 161 (1995)
7. M.C. Nuss, W.H. Knox, U. Koren: Electronics Lett. **32**, 1311 (1996)
8. A.M. Weiner, C.-C. Chang, H.P. Sardesai: OSA Spring Topical Meeting on Ultrafast Electronics and Optoelectronics 1997, paper
9. B. Bouma, G.J. Tearney, S.A. Boppart, M.R. Hee, M.E. Brezinski, J.G. Fujimoto: Optics Lett. **20**, 1486 (1995)
10. I.D. Jung, F.X. Kärtner, N. Matuschek, D.H. Sutter, F. Morier-Genoud, G. Zhang, U. Keller, V. Scheuer, M. Tilsch, T. Tschudi: Optics Lett. **22**, 1009 (1997)
11. M. Nisoli, S. De Silvestri, O. Svelto, R. Szipöcs, K. Ferenz, C. Spielmann, S. Sartania, F. Krausz: Optics Lett. **22**, 522 (1997)
12. A. Baltuska, Z. Wei, M.S. Pshenichnikov, D.A. Wiersma: Optics Lett. **22**, 102 (1997)
13. U. Keller, K.J. Weingarten, F.X. Kärtner, D. Kopf, B. Braun, I.D. Jung, R. Fluck, C. Hönninger, N. Matuschek, J. Aus der Au: IEEE J. Selected Topics in Quantum Electronics **2**, September (1996)
14. D.E. Spence, P.N. Kean, W. Sibbett: Optics Lett. **16**, 42 (1991)
15. U. Keller, G.W. 'tHooft, W.H. Knox, J.E. Cunningham: Optics Lett. **16**, 1022 (1991)
16. F. Salin, J. Squier, M. Piché: Optics Lett. **16**, 1674 (1991)
17. D.K. Negus, L. Spinelli, N. Goldblatt, G. Feugnet: In *Advanced Solid-State Lasers* ed. by G. Dubé, L. Chase, (Optical Society of America, Washington, DC, 1991), Vol 10, p. 120
18. F. X. Kärtner, U. Keller: Optics Lett. **20**, 16 (1995)
19. I.D. Jung, F.X. Kärtner, L.R. Brovelli, M. Kamp, U. Keller: Optics Lett. **20**, 1892 (1995)
20. F.X. Kärtner, I.D. Jung, U. Keller: Special issue on Ultrafast Electronics, Photonics and Optoelectronics, IEEE J. Selected Topics in Quantum Electronics **2**, September (1996)
21. R. Szipöcs, K. Ferencz, C. Spielmann, F. Krausz: Optics Lett. **19**, 201 (1994)
22. F.X. Kärtner, N. Matuschek, T. Schibli, U. Keller, H.A. Haus, C. Heine, R. Morf, V. Scheuer, M. Tilsch, T. Tschudi: Optics Lett. **22**, 831 (1997)
23. U. Keller, D.A.B. Miller, G.D. Boyd, T.H. Chiu, J.F. Ferguson, M.T. Asom: Optics Lett. **17**, 505 (1992)
24. T. Brabec, C. Spielmann, F. Krausz: Optics Lett. **16**, 1961 (1991)
25. J. Zhou, G. Taft, C.-P. Huang, M.M. Murnane, H.C. Kapteyn, I.P. Christov: Optics Lett. **19**, 1149 (1994)
26. R.L. Fork, O.E. Martinez, J.P. Gordon: Optics Lett. **9**, 150 (1984)
27. K. Ferencz, R. Szipöcs: Optical Engineering **32**, 2525 (1993)
28. R. Szipöcs, A. Stingl, C. Spielmann, F. Krausz, F.W. Wise, C.P.J. Barty, (Eds.): In *Generation, Amplification, and Measurement of Ultrashort Laser Pulses II*, Proc. SPIE 1995, paper 11
29. L. Xu, C. Spielmann, F. Krausz, R. Szipöcs: Optics Lett. **21**, 1259 (1996)
30. R. Fluck, I.D. Jung, G. Zhang, F.X. Kärtner, U. Keller: Optics Lett. **21**, 743 (1996)
31. A. Stingl, M. Lenzner, Ch. Spielmann, F. Krausz, R. Szipöcs: Optics Lett. **20**, 602 (1995)
32. U. Keller, T.H. Chiu, J.F. Ferguson: Optics Lett. **18**, 217 (1993)
33. K.J. Weingarten, U. Keller, T.H. Chiu, J.F. Ferguson: Optics Lett. **18**, 640 (1993)
34. R. Fluck, G. Zhang, U. Keller, K.J. Weingarten, M. Moser: Optics Lett. **21**, 1378 (1996)
35. U. Keller: Appl. Phys. B **58**, 347 (1994)
36. B. Braun, C. Hönninger, G. Zhang, U. Keller, F. Heine, T. Kellner, G. Huber: Optics Lett. **21**, 1567 (1996)
37. D. Kopf, F.X. Kärtner, K.J. Weingarten, U. Keller: Optics Lett. **20**, 1169 (1995)
38. J. Aus der Au, D. Kopf, F. Morier-Genoud, M. Moser, U. Keller: Optics Lett. **22**, 307 (1997)
39. C. Hönninger, G. Zhang, U. Keller, A. Giesen: Optics Lett. **20**, 2402 (1995)

40. C. Hönninger, F. Morier-Genoud, M. Moser, U. Keller, L.R. Brovelli, C. Harder: CLEO'97 , paper CMI5 (1997)
41. P.M. Mellish, P.M.W. French, J.R. Taylor, P.J. Delfyett, L.T. Florez: Electronics Lett. **30**, 223 (1994)
42. D. Kopf, K.J. Weingarten, L. Brovelli, M. Kamp, U. Keller: Optics Lett. **19**, 2143 (1994)
43. S. Tsuda, W.H. Knox, E.A d. Souza, W.Y. Jan, J.E. Cunningham: Optics Lett. **20**, 1406 (1995)
44. D. Kopf, A. Prasad, G. Zhang, M. Moser, U. Keller: Optics Lett. **22**, 621 (1997)
45. S. Tsuda, W.H. Knox, S.T. Cundiff: Appl. Phys. Lett. **69**, 1538 (1996)
46. D. Kopf, K.J. Weingarten, G. Zhang, M. Moser, M.A. Emanuel, R.J. Beach, J.A. Skidmore, U. Keller: Appl. Phys. B, to be published Aug. (1997)
47. B.C. Collings, J.B. Stark, S. Tsuda, W.H. Knox, J.E. Cunningham, W.Y. Jan, R. Pathak, K. Bergman: Optics Lett. **21**, 1171 (1996)
48. S. Spälter, M. Böhm, B. Mikulla, A. Sizmann, G. Leuchs, R. Fluck, I.D. Jung, G. Zhang, U. Keller: Appl. Phys. B, accepted (1996)
49. Z. Zhang, K. Torizuka, T. Itatani, K. Kobayashi, T. Sugaya, T. Nakagawa, Optics Lett. **22**, accepted Feb. (1997)
50. H.A. Haus: J. Appl. Phys. **46**, 3049 (1975)
51. H.A. Haus, J.G. Fujimoto, E.P. Ippen: IEEE J. Quantum Electron. **28**, 2086 (1992)
52. H.A. Haus, J.G. Fujimoto, E.P. Ippen: JOSA B **8**, 2068 (1991)
53. F.X. Kärtner, L.R. Brovelli, D. Kopf, M. Kamp, I. Calasso, U. Keller: Optical Engineering **34**, 2024 (1995)
54. C. Spielmann, P.F. Curley, T. Brabec, F. Krausz: IEEE Journal of Quantum Electronics **30**, 1100 (1994)
55. G.P. Agrawal, N.A. Olsson: IEEE Journal of Quantum Electronics **25**, 2297 (1989)
56. L.R. Brovelli, U. Keller, T.H. Chiu: Journal of the Optical Society of America B **12**, 311 (1995)
57. G.P. Agrawal: *Nonlinear Fiber Optics* (Academic Press, New York 1989)
58. I.D. Jung, F.X. Kärtner, J. Henkmann, G. Zhang, U. Keller: Appl. Phys. B **65** 307 (1997)
59. F. Krausz, T. Brabec, C. Spielmann: Optics Lett. **16**, 235 (1991)
60. A. Kasper, K.J. Witte: Optics Lett. **21**, 360 (1996)
61. W.H. Knox, D.S. Chemla, G. Livescu, J.E. Cunningham, J.E. Henry: Phys. Rev. Lett. **61**, 1290 (1988)
62. S.T. Cundiff, W.H. Knox, E.P. Ippen, H.A. Haus: Optics Lett. **21**, 662 (1996)
63. T. Brabec, C. Spielmann, P.F. Curley, F. Krausz: Optics Lett. **17**, 1292 (1992)
64. M. Piché, F. Salin: Optics Lett. **18**, 1041 (1993)
65. I.P. Christov, H.C. Kapteyn, M.M. Murnane, C.P. Huang, J. Zhou: Optics Lett. **20**, 309 (1995)
66. I.D. Jung, L.R. Brovelli, M. Kamp, U. Keller, M. Moser: Optics Lett. **20**, 1559 (1995)
67. L.R. Brovelli, I.D. Jung, D. Kopf, M. Kamp, M. Moser, F.X. Kärtner, U. Keller: Electronics Lett. **31**, 287 (1995)
68. A.E. Siegman: *Lasers* (University Science Books, Mill Valley, Ca 1986)
69. C. Fontaine, P. Requena, A. Munoz-Yagüe: J. Appl. Phys. **68**, 5366 (1990)
70. Z. Shi, H. Zogg, P. Müller, I.D. Jung, U. Keller: Appl. Phys. Lett. **69**, 3474 (1996)
71. G. Cerullo, S. De Silvestri, V. Magni: Optics Lett. **19**, 1040 (1994)
72. M. Lai: Opt. Lett. **19**, 722 (1994)
73. Y.H. Lee, A. Chavez-Pirson, S.W. Koch, H.M. Gibbs, S.H. Park, J. Morhange, A. Jeffery, N. Peyghambarian, L. Banyai, A.C. Gossard, W. Wiegmann: Phys. Rev. Lett. **57**, 2446 (1986)
74. E.O. Göbel: In *Advances in Solid State Physics* ed. by U. Rössler, (Fiedrich Vieweg & Sohn, Braunschweig / Wiesbaden 1990), Vol 30, p. 269
75. P.C. Becker, H.L. Fragnito, C.H.B. Cruz, R.L. Fork, J.E. Cunningham, J.E. Henry, C.V. Shank: Phys. Rev. Lett. **61**, 1647 (1988)
76. J.-Y. Bigot, M.T. Portella, R.W. Schoenlein, J.E. Cunningham, C.V. Shank: Phys. Rev. Lett. **67**, 636 (1991)
77. J. Kuhl, J. Heppner: IEEE Transactions of Quantum Electronics **QE-22**, 182 (1986)
78. P. Laporta, V. Magni: Applied Optics **24**, 2014 (1985)
79. N. Matuschek, F.X. Kärtner, U. Keller: IEEE J. Quantum Electronics **33**, 295 (1997)
80. V. Scheuer, M. Tilsch, T. Tschudi: SPIE Conf. Proc. **2253**, 445 (1994)
81. M. Tilsch, V. Scheuer, T. Tschudi: SPIE Conf. Proc. **2253**, 414 (1994)
82. R.L. Fork, C.H.B. Cruz, P.C. Becker, C.V. Shank: Optics Lett. **12**, 483 (1987)